FATIGUE CRACK GROWTH ON SEVERAL MATERIALS UNDER SINGLE-SPIKE OVERLOADS AND AIRCRAFT SPECTRA

James C. Newman, Jr.[1] and Kevin F. Walker[2]

[1] Mississippi State University, Mississippi, USA (newmanjr@ae.msstate.edu)
[2] QinetiQ Pty Ltd, Melbourne, AUSTRALIA

Abstract: In the mid-1960's, the phenomenon of flat-to-slant crack growth was studied by many in the aircraft industry. At low stress-intensity factors, a fatigue-crack surface is flat (tensile mode) and the crack-front region is under plane-strain conditions (high constraint). As the crack grows with higher stress-intensity factors, a 45-degree shear lip starts to develop at the intersection of the crack front and free surfaces. With further crack extension, a complete shear failure occurs through the thickness of the sheet or plate. This behavior is the shear mode, which is under low constraint or plane-stress conditions. In 1966, Schijve found that the transition from flat-to-slant crack growth on a 2024-T3 Alclad aluminum alloy over a wide range in stress ratios (R) occurred at a "constant" crack-growth rate. Newman and Hudson showed the same behavior on 7075-T6 and Ti 8Al-1Mo-1V alloys, validating Schijve's observation that the crack-growth rate was the key parameter for flat-to-slant crack-growth behavior.

The materials considered herein are 2024-T3, 7075-T6 and 9310 steel. Crack-growth behavior during single-spike overloads and simulated aircraft spectrum loading are presented. The FASTRAN crack-closure based life-prediction code was used to correlate the constant-amplitude crack-growth-rate data over a wide range in stress ratios (R) and rates from threshold to fracture, and to calculate or predict the crack-growth behavior on single-spike overload tests. Crack-closure behavior is strongly dependent upon the level of constraint. The main objective was to see if the constraint-loss region is the primary reason for crack-growth delays after single-spike overloads. Also, crack-growth analyses are presented on tests that were conducted by Wanhill on 2024-T3 Alclad aluminum alloy under the TWIST (standard European) transport wing spectrum. Crack-growth analyses using crack-closure theory without constraint loss was "unable" to predict crack growth under spike overloads or simulated aircraft spectra. However, predicted crack length against cycles with constraint-loss behavior compared reasonably well with all tests.

Keywords: Cracks, stress-intensity factor, crack growth, crack closure, plasticity, spectra

INTRODUCTION

Fatigue-crack growth in metallic materials has been studied for the past 70 years. The Comet airplane failures in the mid-1950's was instrumental in starting research programs world-wide by many aircraft companies and universities to understand the controlling factors. The development of the principles of Fracture Mechanics, especially the crack-tip stress-intensity factor (K), has provided aircraft designers with a methodology to predict fatigue lives and fatigue-crack growth lives of complex metallic components. In the mid-1960's, the phenomenon on flat-to slant crack growth, as shown in Figure 1, was studied by many in the aircraft industry [1]. At low stress-intensity factors, a crack surface is very flat, and the behavior is referred to as the tensile crack-growth mode. In addition, the stress state in the crack-front region is under plane-strain conditions or what is called high constraint. As the crack grows with higher stress-intensity factors, a 45-degree shear lip starts to develop at the intersection of the crack front and the free surfaces. At a certain point, with further crack extension, a complete shear failure occurs through the thickness of the sheet or plate. This behavior is the shear mode, which is under low constraint or plane-stress conditions.

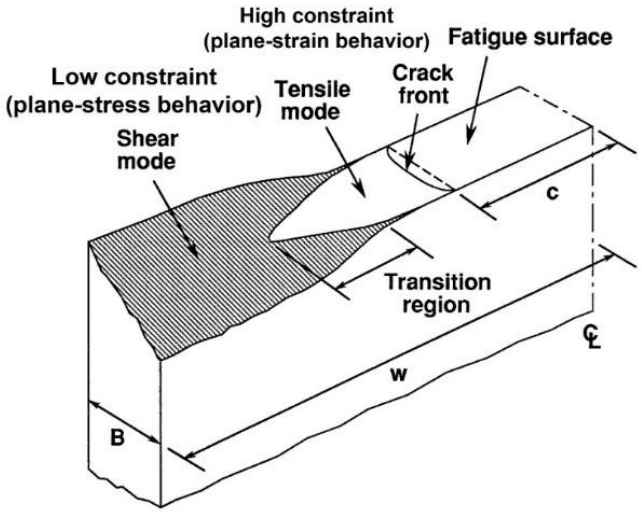

Figure 1: Schematic of flat-to-slant fatigue-crack growth in metallic materials.

In 1966, Schijve [2] found that the transition from flat-to-slant crack-growth behavior in a 2024-T3 alloy occurred at a "constant" crack-growth rate, independent of R. Others at the ASTM Symposium on Crack Propagation [1] had proposed that ΔK or K_{max} controlled the transitional behavior. Newman [3] in a discussion on the subject provided additional test data from the NASA Langley Research Center by Hudson on 7075-T6 [4] and Ti 8Al-1Mo-1V [5] alloys to support Schijve's conclusion that crack-growth rate was the controlling parameter.

In studying fatigue-crack growth behavior in a 2024-T3 aluminum alloy, Elber [6] discovered the crack-closure phenomenon, whereby the crack surfaces are partially closed under tensile loading. Cracks only grow when the crack tip is fully open. He proposed that the effective stress-intensity factor, ΔK_{eff}, controlled the fatigue-crack-growth rates as

$$\Delta K_{eff} = (S_{max} - S_o) \sqrt{(\pi\ c)}\ F \tag{1}$$

where S_{max} is the maximum remote applied stress, S_o is the crack-opening stress, c is crack half-length, and F is the boundary-correction factor. The plasticity-induced crack closure (PICC) concept has revolutionized the analyses of crack growth under constant- and variable-amplitude loading. Elber found that the measured crack-opening values at various stress ratios ($R = S_{min}/S_{max}$) was able to collapse the crack-growth-rates onto a nearly unique relation between ΔK_{eff} and rate.

PLANE-STRAIN TO PLANE-STRESS FATIGUE-CRACK-GROWTH BEHAVIOR

Since Schijve showed that flat-to-slant crack growth occurred at a constant rate (dc/dN), then Elber's relation would indicate that ΔK_{eff} controls the flat-to-slant (plane-strain to plane-stress) crack-growth region. In 1992, Newman [7] developed a relation to predict the flat-to-slant crack-growth location as

$$(\Delta K_{eff})_T = 0.5\ \sigma_o\ \sqrt{B} \tag{2}$$

where σ_o is the flow stress (average between the yield stress and ultimate tensile strength) and B is sheet or plate thickness. However, as shown in Figure 1, the change from flat (plane strain) to slant (plane stress) is not sudden and occurs over a transition range. During the transition, the constraint condition is neither plane strain nor plane stress, but is somewhere in between. This transitional region is called the constraint-loss regime (CLR). Previous work [7, 12, 13] has determined the CLR by trial-and-error methods using spectrum loading tests. For the current work it was considered that single-spike overload and underload tests in addition to spectrum loading tests may be a better way to establish the CLR.

FATIGUE-CRACK-GROWTH AGAINST ΔK_{eff} CORRELATIONS

The FASTRAN crack-closure model [8] was used to develop the ΔK_{eff}-rate relations for several materials used in this study, such as 2024-T3, 7075-T6, and 9310 steel.

Aluminum Alloy: 2024-T3 Sheet (Bare)

Crack-growth results from Hudson [4], Dubensky [9] and Phillips [10] on middle-crack tension, M(T), specimens made of 2024-T3 aluminum alloy sheet (thickness B = 2.3 mm) are shown in Figure 2. The figure shows elastic ΔK_{eff} plotted against crack-growth rate. The data collapsed into a narrow band for all stress ratios. Some large differences occurred during the high stress ratio, R, tests in the high-rate regime. These tests were conducted on the 305-mm wide specimens at extremely high stress levels (0.75 and 0.95 of the yield stress). Even elastic-plastic analyses were unable to collapse these data along a unique curve in this region. However, the elastic-plastic fracture criterion (Two-Parameter Fracture Criterion, see Newman [11]) used in the analysis (K_F = 267 MPa$\sqrt{m}$; m = 1) predicted failure very near to the vertical asymptotes of these tests, see the vertical dashed lines. Note that the TPFC analysis accounts for specimen width, with the wider specimen approaching fracture at higher values of applied stress-intensity range and associated crack growth rate.

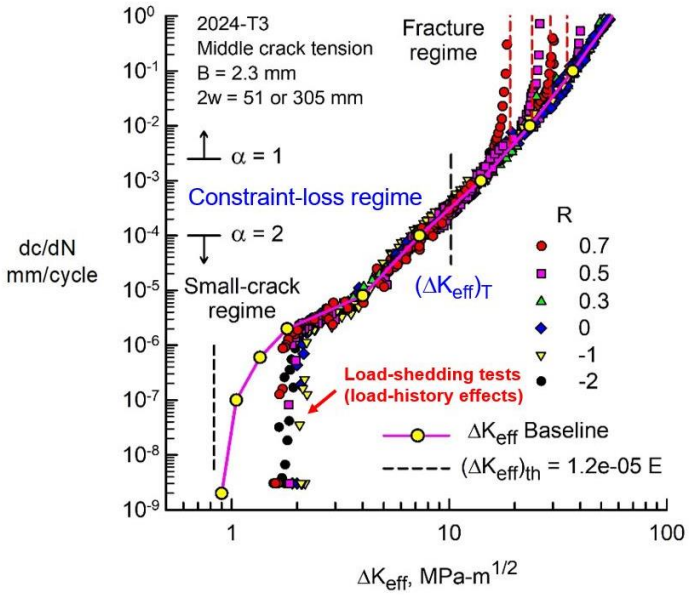

Figure 2: Effective stress-intensity factor against rate for 2024-T3 bare M(T) specimens.

A constraint factor (α) of 2.0 was found to coorelate the rates in terms of ΔK_{eff} for rates less than 1E-04 mm/cycle and α equal to 1.0 was used for rates greater than 2.5E-03 mm/cycle. These low-rate data were determined from the 51-mm wide specimens. For intermediate rates, α was varied linearly with the logarithm of crack-growth rate [12,13]. The values of α and rate were selected by trial-and-error and from analyses of crack growth under spectrum loading [7]. For the 2024-T3 alloy sheet, $(\Delta K_{eff})_T$ = 10.2 MPa$\sqrt{m}$, a value which falls within the constraint-loss regime.

In the low crack-growth rate regime, near the large-crack threshold, tests and analyses have shown that thresholds develop because of a rise in the crack-opening stresses due to the load-shedding procedure (see Newman [14]). In the threshold regime then, the actual ΔK_{eff} -rate data would lie at lower values of ΔK_{eff} because the rise in crack-opening stress was not accounted for in the current analysis. For the present study, an estimate was made for this behavior on the basis of small-crack data (see Newman and Edwards [15]) and it is shown by the solid line below rates of about 2E-06 mm/cycle. The vertical dashed line in the small-crack regime shows an estimate for the effective stress-intensity-factor threshold, $(\Delta K_{eff})_{th}$, based on the modulus of elasticity [16].

Aluminum Alloy: 7075-T6 Sheet (Bare)

Herein, the results of fatigue-crack-growth tests made on M(T) specimens are compared with previous test data from NASA Langley Research Center on the same material [4, 17] in the constraint-loss region (CLR). Figure 3 shows ΔK against crack-growth rate (dc/dN) for R = 0 loading. The new test data (solid symbols) compared well over more than 2-orders of magnitude in rates. The two horizontal lines show the start and end of the estimated CLR that was determined many years ago by trial-and-error procedures. The light grey symbols are ΔK_{eff} data determined from a crack-monitoring system [18] using the zero-percent compliance offset values from the two low-R tests. The measured ΔK_{eff}-rate data agreed well with the ΔK_{eff} curve (blue lines with yellow symbols) previously established [19].

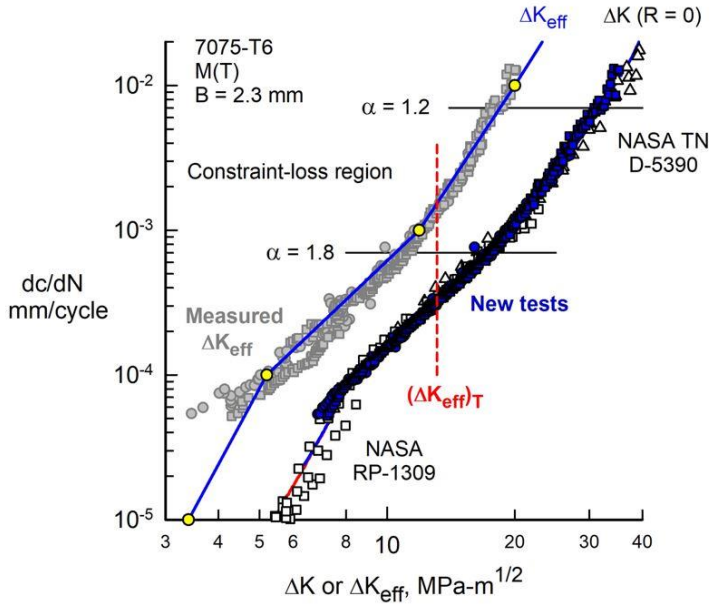

Figure 3: Stress-intensity factor against rate for 7075-T6 bare M(T) specimens.

The current tests at R = 0 loading were designed to propagate the crack across the CLR. Crack length and crack-opening loads were measured from the crack-monitoring system [18] using crack-mouth-opening-displacement (CMOD) gauges. Again, the zero-percent compliance offset values were determined from the 1 and 2% offset values as OP0 = 2 OP1 – OP2. (OPn is the compliance offset value at n-percent [19].) Figure 4 shows P_o/P_{max} plotted against the c/w ratio. The horizontal dashed lines show the crack-opening-load ratio for plane-strain (α = 3) and plane-stress (α = 1) behavior. Tests B1

and B5 were tested at S_{max} = 50 MPa and R = 0.1 at 0.5 hz, which showed a rise in the crack-opening ratio for c/w > 0.55. The very low frequency was used to reduce the mechanical noise from the CMOD gauges to improve crack-opening load measurements. Measurements of P_o/P_{max} from the experiments showed large scatter but showed the correct trend. The curve was calculated crack-opening-load ratios from FASTRAN [13] using the current constraint-loss regime (see Fig. 3).

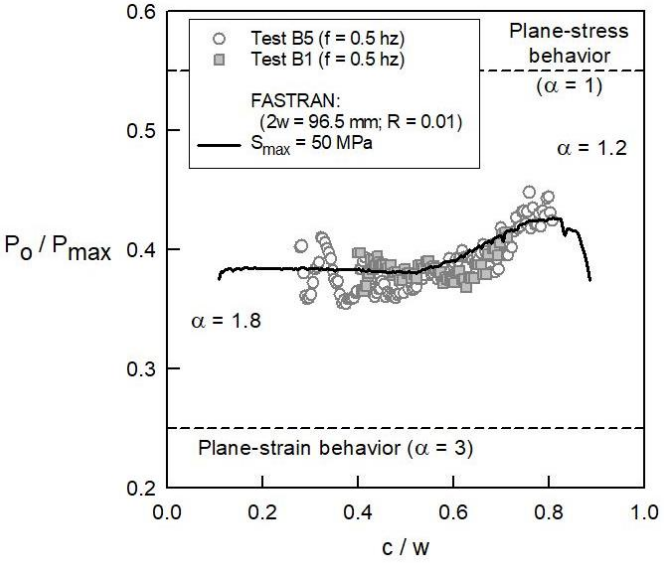

Figure 4: Stress-intensity factor against rate for 7075-T6 sheet M(T) specimens.

Steel: 9310 Plate

Compact, C(T), specimens were used to generate the ΔK against rate (dc/dN) data on the 9310 steel at room temperature and 20 Hertz [21, 22] over a wide range in stress ratios (R = 0.1 to 0.95). Tests were conducted from near threshold to fracture. A backface strain (BFS) gauge was used to monitor crack growth and to measure crack-opening loads using the compliance-offset method. In the low-rate regime, compression pre-cracking constant amplitude (CPCA) and load reduction (CPLR) methods were used to generate ΔK-rate data [23, 24] to minimize load-history effects from the load-shedding method [20].

A crack-closure analysis was then performed on the fatigue-crack growth (ΔK-rate) data from C(T) specimens to determine the ΔK_{eff}-rate relation. The K-analogy concept [12, 13] was used to calculate the crack-opening stresses (or loads) for C(T) specimens. The ΔK_{eff}-rate data are shown in Figure 5.

Selection of the lower constraint factor, 2.5, was found to reasonably collapse the ΔK-rate data onto an almost unique relation. In the threshold region, the lower R tests exhibited a rise in crack-opening loads as the ΔK level was reduced in a load-reduction test. Even the CPLR method showed a load-history effect, but not as much as the current ASTM procedure [20]. The upper constraint factor, 1.15, and constraint-loss range was selected to help fit spectrum crack-growth tests [25]. The lower vertical dashed line at $(\Delta K_{eff})_{th}$ is the estimated threshold for the steel [16]; and the upper vertical dashed line at $(\Delta K_{eff})_T$ is the location of constraint loss from plane-strain to plane-stress behavior [7] calculated from Equation (2). The solid (blue) lines with circular (yellow) symbols shows the baseline crack-growth-rate curve for FASTRAN.

The test data at high rates shown in Figure 5 illustrates an issue with the test-specimen width. Small width specimens may fracture during or before the CLR, which makes it difficult to establish the region. Large width specimens were used to generate the test data shown in Figure 2 and the CLR was transitioned in a stable manner before fracture. Small test specimens are satisfactory for low rates near threshold, but large width specimens are needed to generate test data at high rates and fracture toughness.

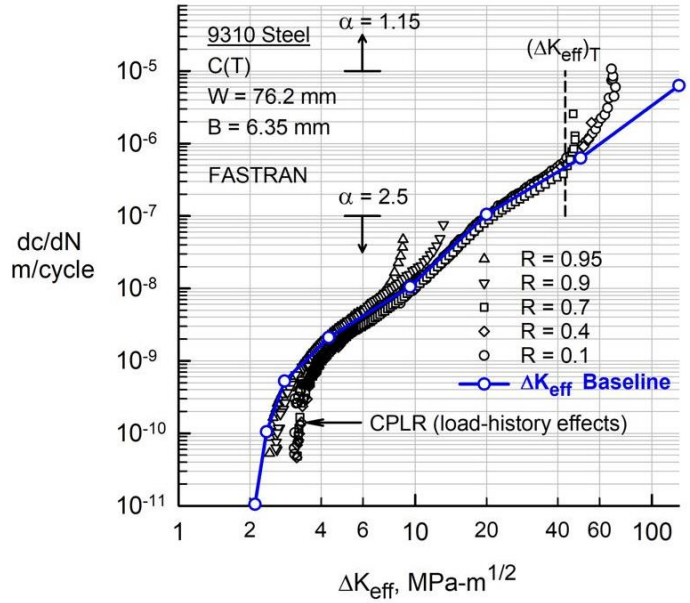

Figure 5: Effective stress-intensity factor against rate for 9310 steel C(T) specimens.

SINGLE-SPIKE OVERLOAD/UNDERLOAD TESTS AND ANALYSES

The loading sequence that was applied during single-spike overload/underload testing is shown in Figure 6. A crack was grown from the crack-starter notch under constant-amplitude (CA) loading at a given maximum load level and R for N_{CA} cycles. A single-spike overload at OL value was statically applied, and then an under load at UL value was applied. CA loading continued until steady-state behavior was achieved. Then another OL and UL was applied, and the crack grown under CA loading to a specified crack length. The specimen was then statically pulled to failure to determine the fracture toughness.

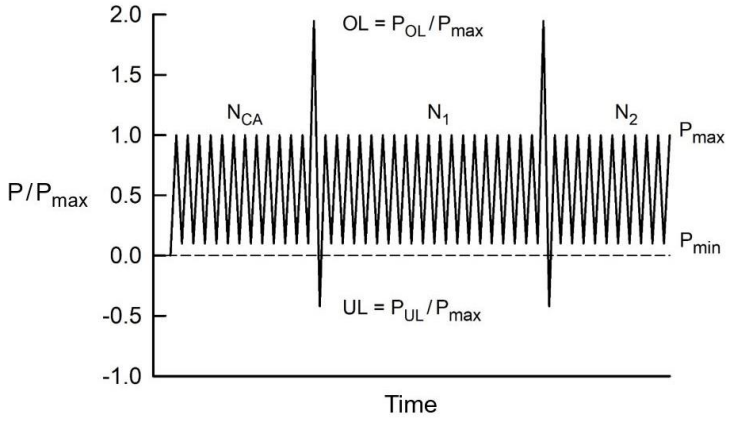

Figure 6: Single-spike overload and underload sequence under constant-amplitude loading.

Aluminum Alloy: 2024-T3 Plate

Yisheng and Schijve [26] conducted single-spike overload and underload tests on M(T) specimens 6.35 mm-thick and 105 mm-wide, made from 2024-T3 aluminum alloy. In one specimen, a crack was grown from an initial size of 3 mm to c = 6 mm under 76,000 cycles at S_{max} = 100 MPa and R = 0 constant-amplitude (CA) loading. At this point, a 200 MPa overload (S_{OL}) was applied and the test was continued at the previous constant-amplitude loading. During these tests, the crack-length-against-cycles and crack-opening stresses were measured during and after the overload. Measured and predicted crack-length-against-cycles from the test is shown in Figure 7. Note that the predicted cycles have been shifted in order to match crack length and cycles at the initial crack length (solid symbol). The solid (black) curve shows crack-growth predictions made in 1997 using FASTRAN Version 3.0 [27], which used

block loading (NMAX = 300) to speed-up calculations. Recently, FASTRAN Version 5.76 (cycle-by-cycle calculations) was used to make the same predictions and the results are shown as the solid (blue) curve, which agreed better with the test data. The same CLR was used in both predicitons. To illustrate the influence of the CLR, a prediction was made using "constant" constraint (α = 2) and these results are shown as the dashed (blue) curve, which showed very little influence of the overload.

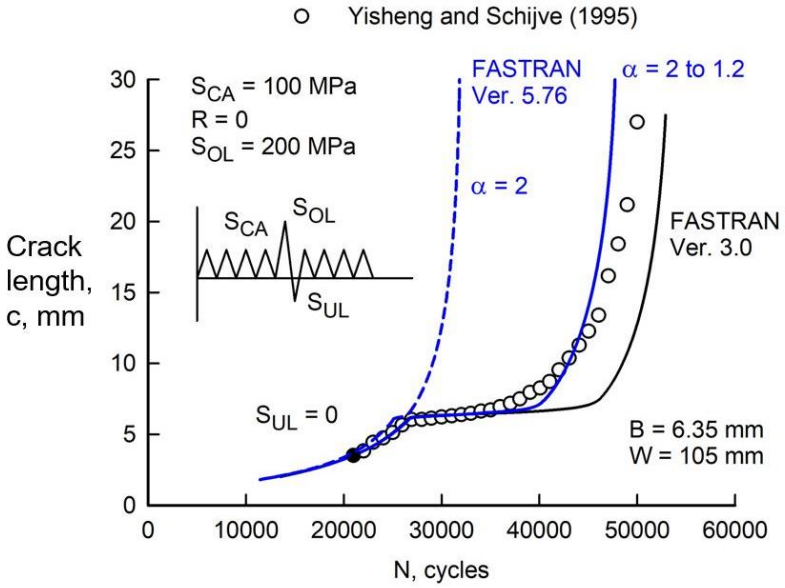

Figure 7: Measured and predicted crack-length-against-cycles under a single-spike overload.

These results illustrate that the overload activated the large plastic-zone size (α = 1.2) and caused more crack-growth delay. The plastic-zone size was about a factor of 2.8 times larger than that calculated with α = 2.

A comparison of measured and predicted crack-opening stresses for the single-spike overload test is shown in Figure 8. The predicted results using both FASTRAN versions agreed reasonably well with the measured trends. The model tended to predict slightly lower values during the constant-amplitude portion but predicted slightly higher crack-opening stresses after the overload. The length of influence of the overload in terms of cycles, however, was predicted well by both models. These test results and analyses occurred almost exclusively in the CLR (α varied from 2 to 1.2). The saw-tooth nature of the calculated results are due to the lumping procedure used to eliminate elements in the model to maintain model efficiency and speed. The difference between the predicted crack-opening stresses (solid curve) and the dashed line (S_{CA}) gives the effective stress range that is used to compute the effective stress-intensity factor range and, thus, the crack-growth rate.

Aluminum Alloy: 2024-T3 Sheet (Bare)

For the 305-mm wide thin-sheet 2024-T3 alloy, the end of the esitmated CLR is well below the crack-growth rate at fracture, see Figure 2. However, fracture tests are needed on smaller width specimens to accurately predict failure so that crack-growth tests can be designed to generate test data at higher rates while avoiding the fracture regime as much as possible. Anti-buckling guide plates were used in the fracture tests to help prevent buckling. The elastic stress-intensity factor, K_{Ie}, at fracture is plotted against c_i/w ratio in Figure 9. Circular symbols are test data from Newman [28] on larger width specimens and square symbols are tests conducted on 96.5-mm width M(T) specimens. The wider specimens failed at larger values of K_{Ie} than the smaller width specimens. Solid and dashed curves in Figure 9 are the calculated K_{Ie} at failure from the TPFC for net-section stresss (S_n) less or greater than the proportional limit of the material (σ_{pl}), respectively. For S_n less than σ_{pl}, $K_F = K_{Ie}/(1 - m\, S_n/\sigma_u)$ and for $S_n > \sigma_{pl}$, a more complicated equation was developed [28]. In the TPFC, the fracture toughness

parameter m = 0 for linear-elastic fracture mechanics (brittle fracture) and m = 1 for very ductile materials. For the thin-sheet aluminum alloy, the elastic-plastic fracture toughness was determined to be K_F = 267 MPa-$m^{1/2}$ and m = 1. (Ouidadi [29] using an elastic-plastic finite-element analysis with the critical crack-tip-opening-angle (CTOA) failure criterion on an aluminum alloy validated the TPFC. Her work indicated that the seperation between linear and non-linear fracture behavior in the TPFC equations was the proportional limit and not the yield stress of the material.)

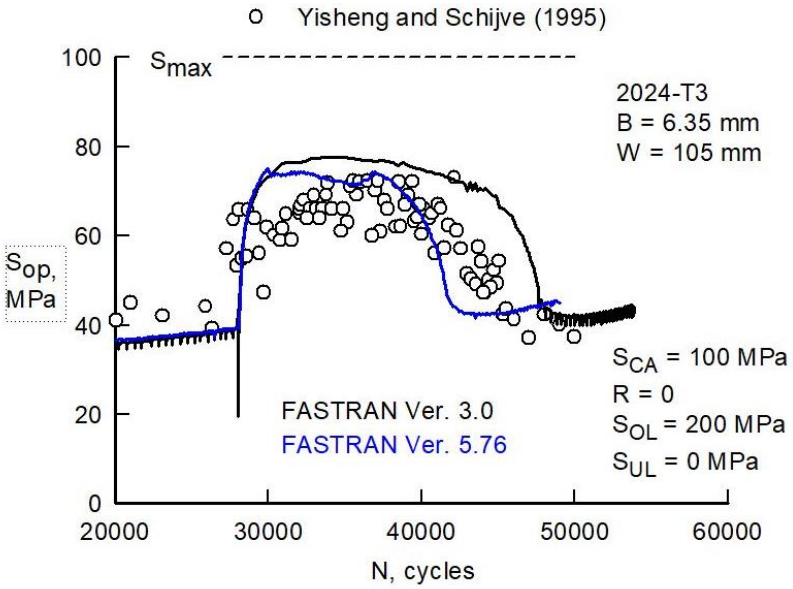

Figure 8: Measured and predicted crack-opening stress under a single-spike overload.

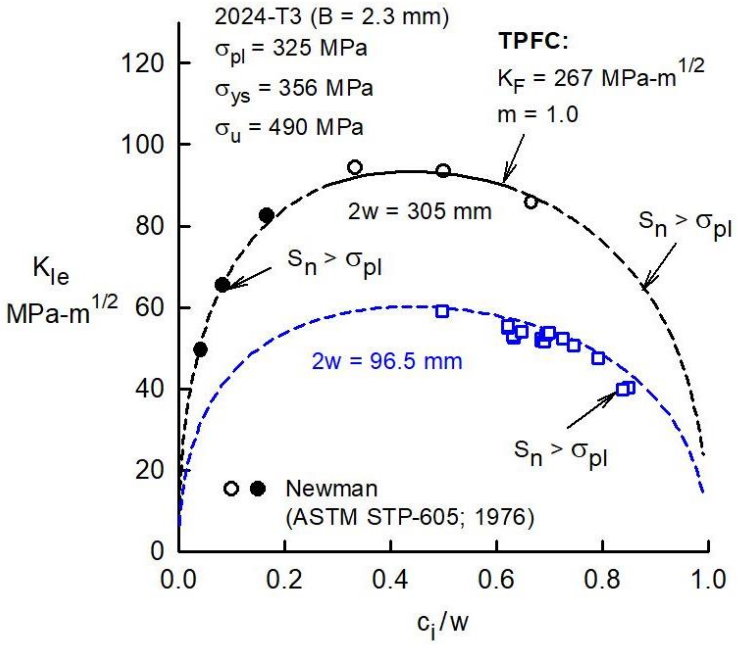

Figure 9: Measured and calculated elastic fracture toughness for 2024-T3 (Bare) alloy.

The results of a repeated single-spike overload/underload test (solid circular symbols) are shown in Figure 10 on a 2024-T3 M(T) specimen. Test A4 was subjected to S_{max} = 55 MPa at R = 0.01 loading and a frequency (f) of 2 hz after 20,000 compression cycles at S_{max} = 0 and S_{min} = - 70 MPa. The crack was initiated at the crack-starter notch (c_n = 9 mm) and grown to c = 14 mm. Here, a factor of 2 overload (110 MPa) was statically applied and then unloaded to zero (UL = 0). CA loading resumed and the crack was grown to 19 mm, where another factor of 2 overload was applied.

FASTRAN Version 5.76 [13] was used to predict crack growth using the ΔK_{eff}-rate curve (see Fig. 2) and the CLR that had previously been determined for the thin-sheet alloy. The dashed curve is under CA loading while the solid (blue) curve is under the repeated spike overload/underload test. The model predicted the crack-growth delay from the first and second overloads reasonable well. The dash-dot curve shows the results for constant constraint (α = 2), which predicted very little crack-growth delay after both overloads.

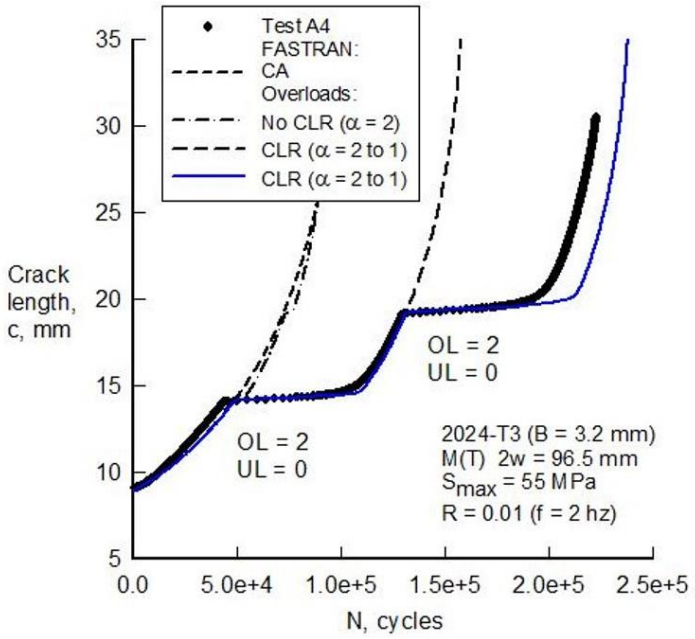

Figure 10: Measured and predicted crack-length-against-cycles under a single-spike overload.

Aluminum Alloy: 7075-T6 Sheet (Bare)

Herein, the results of fracture tests conducted on smaller width M(T) specimens are compared with previous tests on wider M(T) specimens from the NASA Langley Research Center on the same material. The elastic stress-intensity factor, K_{Ie}, at fracture is plotted against c_i/w ratio in Figure 11. Circular symbols are test data from Hudson [4] on larger width (305-mm) specimens and the square symbols are tests conducted herein on 96.5-mm width M(T) specimens. The wider specimens failed at larger values of K_{Ie} than the smaller width specimens. For the thin-sheet aluminum alloy, the elastic-plastic fracture toughness was determined to be K_F = 124 MPa-$m^{1/2}$ and m = 0.85. Solid and dashed curves are calculated K_{Ie} values at failure from the TPFC for net-section stressses (S_n) less or greater than the proportional limit of the material (σ_{pl}), respectively. The larger width specimens showed more scatter than the smaller width specimens, but 70% of the failure values were within +/- 5% of the solid curve.

The results of a repeated single-spike overload/underload test (solid circular symbols) are shown in Figure 12 on a 7075-T6 M(T) specimen. Test B8 was subjected to S_{max} = 75 MPa at R = 0.01 loading and a frequency (f) of 2 hz after 20,000 compression cycles at S_{max} = 0 and S_{min} = - 70 MPa. The crack was initiated at the crack-starter notch (c_n = 5 mm) and grown to c = 10 mm. Here, a factor of 2 overload (150 MPa) was statically applied and then unloaded to zero (UL = 0). CA loading resumed and the crack was grown to 15 mm, where another factor of 2 overload was applied.

Again, FASTRAN Version 5.76 [13] was used to predict crack growth using the ΔK_{eff}-rate curve (see Fig. 3) and the CLR that had previously been determined for the thin-sheet alloy. The dashed curve is under CA loading while the solid (blue) curve is under the repeated spike overload/underload test. The model over predicted the delay from the first overload but was reasonable for the second overload. These results suggest that the start of the CLR needs to be moved to a slightly higher rate, so that less

delay would occur. The dash-dot curve shows the results for constant constraint (α = 1.8), which predicted very little crack-growth delay after both overloads.

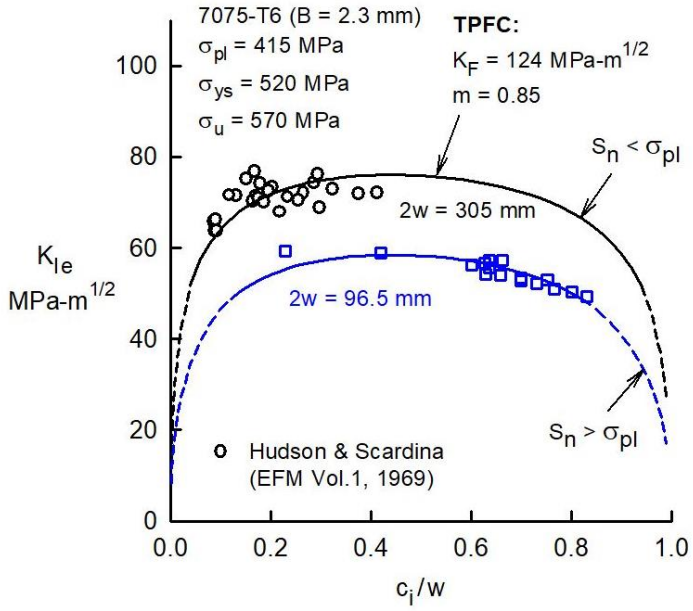

Figure 11: Measured and calculated elastic fracture toughness for 7075-T6 (Bare) alloy.

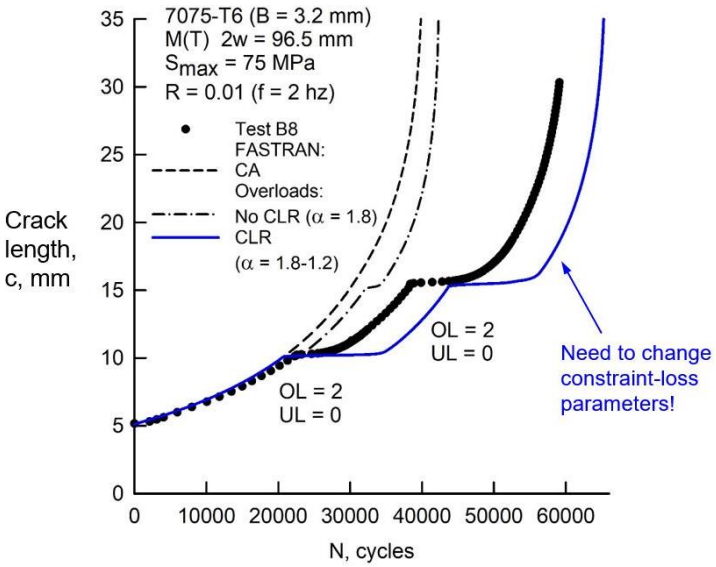

Figure 12: Measured and predicted crack-length-against-cycles under a single-spike overload.

Steel: 9310 Plate

The results of a repeated single-spike overload/underload test (open circular symbols) are shown in Figure 13 on a 9310 steel C(T) specimen. The specimen was subjected to $S_{max} = P_{max}/(WB)$ = 10.7 MPa at R = 0.1 loading with a frequency (f) of 18 hz after compression pre-cracking. The crack was initiated at the crack-starter notch and grown to c = 39 mm under CA loading. Here, a factor of 2 overload was statically applied and then unloaded to zero load. CA loading was resumed and the crack was grown to 54 mm, where another factor of 2 overload was applied.

FASTRAN Version 5.33 [12] was used to predict crack growth using the ΔK_{eff}-rate curve (see Fig. 5) and the CLR that had previously been determined [25]. The dashed curve is under CA loading while

the solid (blue) curve is under the repeated spike overload/underload test. Here the overloads were applied on the basis of cycles instead of crack length. The model predicted the slight delay from the first overload but was reasonable for the second overload. The dashed curve shows the results of constant constraint (α = 2.5), which predicted very little crack-growth delay after the overloads.

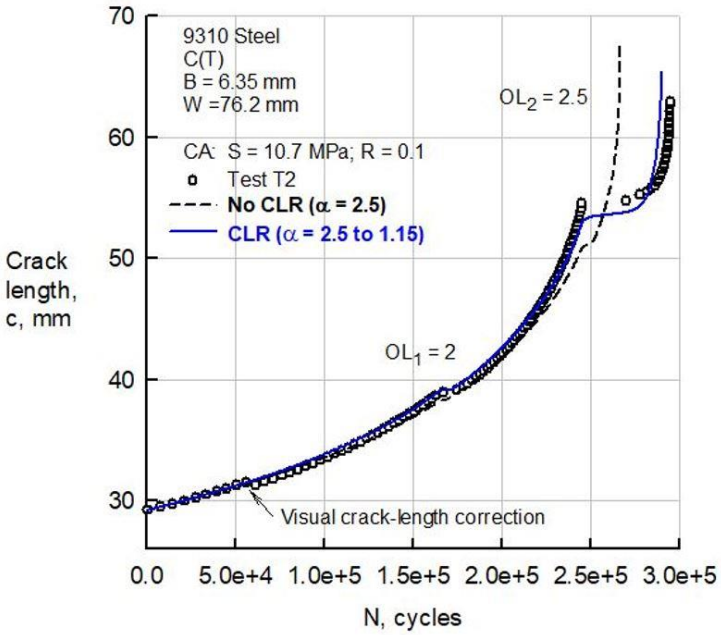

Figure 13: Measured and predicted crack-length-against-cycles under a single-spike overload.

AIRCRAFT SPECTRUM LOADING TESTS AND ANALYSES

As pointed out by Wanhill and Schijve [30], the ability to predict crack-growth behavior under the TWIST [31] spectrum loading has eluded the empirical crack-growth (retardation and acceleration) models in the literature. However, the strip-yield models, such as those developed by Dill and Saff [32], Fuhring and Seeger [33], Newman [8], and de Koning and Liefting [34] probably have a reasonable chance of predicting such behavior. These models have numerical "memory" to account for the occurrence of overloads, underloads and overlapping plastic zones and should be able to characterize the plastic and residual plastic deformation histories generated under the TWIST spectrum. As will be presented later, the constraint factor plays a leading role in allowing the strip-yield model to predict the crack-opening stress history that develops under the TWIST spectrum. In the following sections, the closure model will be used with the baseline ΔK_{eff}-rate relations, previously determined, to calculate crack growth in a 2024-T3 Alclad aluminum alloy sheet material under a clipped version of the TWIST spectrum.

Wanhill [35, 36] conducted spectrum crack-growth tests on M(T) specimens made of 2024-T3 Alclad material in two thicknesses (B = 1.6 and 3.1 mm). Only the results on the thicker material will be shown herein. Crack-length-against-flight data on the 3.1 mm-thick specimens tested under the TWIST (Level III) loading are shown in Figure 14 as open symbols. Tests were conducted at a mean stress level of S_{mf} = 70 MPa. The initial crack starter notch half-length was 3.5 mm. Comparisons are made between experimental and predicted crack length against flights.

The solid curve is the calculated results from the closure model with the variable-constraint condition (α = 2 to 1) using the baseline ΔK_{eff}-rate relation [7]. Using the CLR established for the aluminum alloy and the model, the predicted results agreed well with the tests (within 15 percent). To illustrate why the variable-constraint conditions are necessary, example calculations are made for constant constraint conditions of either α = 1 or 2 (dashed-dot curves). The model with a low constraint

condition (α = 1) predicted slightly longer flights to a given crack length than the test data for the thin material but predicted much longer lives for the thick material.

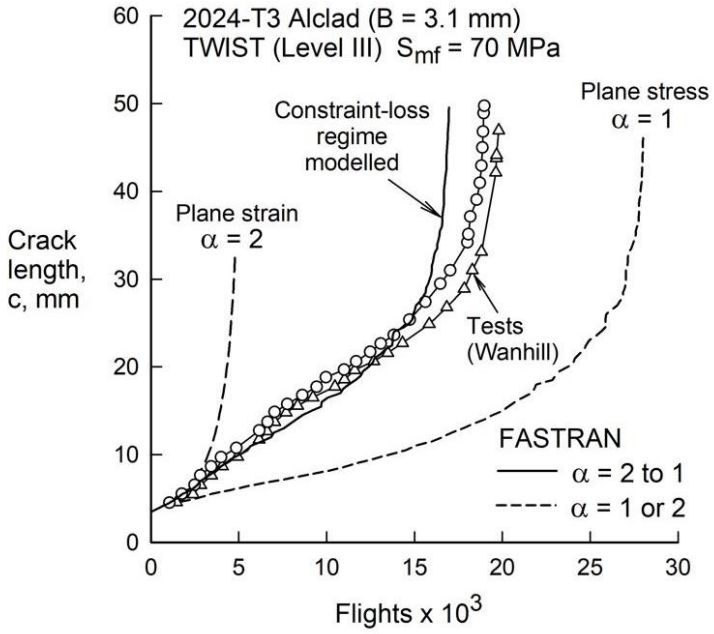

Figure 14: Measured and predicted crack-length-against-cycles under a single-spike overload.

CONCLUDING REMARKS

The phenomenon of flat-to-slant crack growth has been associated with plane-strain to plane-stress crack-growth behavior. For a structural component with a crack growing under pure plane-strain (α = 3) conditions (flat crack surfaces) and then subjected to an overload that is large enough to activate constraint loss under plane-stress (α = 1) conditions, the crack front develops a plastic-zone size nearly an order-of-magnitude larger than under plane-strain conditions. The larger plastic-zone size would greatly influence crack-growth behavior and the increased crack-closure behavior would cause much more crack-growth delay.

Schijve's discovery that the transition from flat-to-slant crack growth occurred at a "constant" crack-growth rate and Elber's discovery of plasticity-induced crack closure lead to the development of the transition being expressed in terms of ΔK_{eff}, sheet or plate thickness, and material stress-strain properties.

The materials considered herein are 2024-T3 (Alclad and bare), 7075-T6 (bare) and 9310 steel. Crack growth during single-spike overload behavior and simulated aircraft spectrum loading were presented. The FASTRAN crack-closure based life-prediction code was used to correlate the constant-amplitude crack-growth-rate data over a wide range in stress ratios (R) and rates from threshold to fracture, and to calculate or predict the crack-growth behavior on the single-spike overload tests. Also, crack-growth analyses are presented on tests that were conducted by Wanhill on 2024-T3 Alclad aluminum alloy under the TWIST (standard European) transport wing spectrum. Crack-growth analyses using crack-closure theory without constraint loss was unable to predict crack growth under spike overloads or simulated aircraft spectra. However, predicted crack length against cycles with constraint-loss behavior compared reasonably well with all tests.

REFERENCES

[1] Fatigue Crack Propagation (1967). ASTM STP 415, American Society for Testing Materials, Philadelphia, PA.
[2] Schijve, J. (1967). In: *Fatigue Crack Propagation*, ASTM STP 415, p. 415.
[3] Newman, J. C., Jr. (1967). In: *Fatigue Crack Propagation*, ASTM STP 415, p. 380.
[4] Hudson, C. M. (1969). NASA TN D-5390.
[5] Hudson, C. M. (1965). NASA TN D-2743.
[6] Elber, W. (1971). ASTM STP 486, p. 230.
[7] Newman, J. C., Jr. (1992). In: *Fatigue of Aircraft Materials*, A. Beukers et al., eds., Delft University Press, p. 83.
[8] Newman, J. C., Jr. (1981). In: *Methods and Models for Predicting Fatigue Crack Growth under Random Loading*, eds. J. B. Chang and C. M. Hudson, ASTM STP 748, p. 53.
[9] Dubensky, R. G. (1971). NASA CR-1732.
[10] Phillips, E. P. (1988). In: *Mechanics of Fatigue Crack Closure*, eds. J. C. Newman, Jr. and W. Elber, ASTM STP 982, p. 505.
[11] Newman, J. C., Jr. (1976). In: *Properties Related to Fracture Toughness*, ASTM STP 605, p. 104.
[12] Newman, J. C., Jr. (1992). NASA TM 104159.
[13] Newman, J. C. Jr. (2013). FASTRAN Version 5.4 User Guide, Fatigue and Fracture Associates LLC, Eupora, MS, USA.
[14] Newman, J. C., Jr. (1983). In: Behaviour of Short Cracks in Airframe Components, ed. H. Zocher. AGARD CP-328, p. 6.1-6.26.
[15] Newman, J. C., Jr. and P. R. Edwards, P. R. (1988). AGARD R-732.
[16] Newman, J. C., Jr.; Kota, K. and Lacy, T.E. (2018). *Eng. Fract. Mech.*, vol. *187*, p. 211.
[17] Newman, J. C., Jr., Wu, X. R., Venneri, S. L. and Li, C. G. (1994). NASA RP-1309.
[18] Donald, J. K. and Blair, A. (2009) Automated Fatigue Crack Growth Testing and Analysis – Series 2001. Ver. 3.09, Fracture Technology Associates, LLC, Bethlehem, PA.
[19] Newman, J.C., Jr. and Walker, K. F. (2019). *Theo. & Appl. Fract. Mech.*, vol. 100, p. 307.
[20] Standard Test Method for Measurement of Fatigue Crack Growth Rates. (2016). ASTM E-647.
[21] Newman, J. C., Jr.; Vizzini, A. and Yamada, Y. (2010). Department of Transportation, DOT/FAA/AR-10/3, Washington, D.C., USA.
[22] Newman, J.C. Jr. (2021). *Metals* vol. 11.
[23] Yamada, Y. and Newman, J.C. Jr. (2009) *Eng. Fract. Mech.*, vol. 76, p. 209.
[24] Yamada, Y. and Newman, J.C. Jr. (2009). *Int. J. Fatigue*, vol. 31, p. 1780.
[25] Newman, J.C. Jr.; Yamada, Y.; Ziegler, B.M. and Shaw, J.W. (2014). Department of Transportation, DOT/FAA/TC-13/29, Washington, D.C., USA.
[26] Yisheng Wu and Schijve, J. (1995). *Fat. Fract. Eng. Mat. Struc.,* vol. 18, p. 917.
[27] Newman, J. C., Jr. (1997). In: High Cycle Fatigue of Structural Materials, W. O. Soboyejo and T. S. Srivatsan, eds., The Minerals, Metals & Materials Society, p. 109.
[28] Newman, J. C., Jr. (1976). In: Properties Related to Fracture Toughness. ASTM STP 605, p. 104.
[29] Ouidadi, H. (2017). MS Thesis, Mississippi State University, USA.
[30] Wanhill, R. J. H. and Schijve, J. (1988). NLR MP 88001 U.
[31] de Jonge, J. B., Schutz, D., Lowak, H. and Schijve, J. (1973). LBF-Bericht FB-106 & NLR TR 73029 U.
[32] Dill, H. D. and Saff, C. R. (1976). ASTM STP 595, p. 306.
[33] Fuhring, H. and Seeger, T. (1979). ASTM STP 677, p. 144.
[34] de Koning, A. U. and Liefing, G. (1988). ASTM STP 982, p. 437.
[35] Wanhill, R. J. H. (1977). NLR TR 77092 U.
[36] Wanhill, R. J. H. (1979). *Fat. Eng. Mater. Struct.*, vol. 1, 1979, p. 5.